



**Scientific-Research Article**

**Effects of harmonic control and dynamic twist on helicopter rotor performance in forward flight**

Farid Shahmiri<sup>1\*</sup>, Fatemeh Kiani<sup>2</sup>

1-2- Aerospace Engineering Department, University of Technology Malek Ashtar, Tehran, Iran

**ABSTRACT**

**Keywords:** Helicopter performance, Blade dynamic twist, Higher Harmonic Control, Desirability approach

The optimum rotor blade planform of helicopters required to minimize power, maximize rotor thrust, and maximize lift-to-drag ratio in forward flight, using a numerical optimization approach, is investigated. Here, the traditional approach is modified by Central Composite Design (CCD) and a flight dynamic simulation program coupled with a desirability optimization technique implemented in the process of blade optimization. The optimum blade planform parameters (i.e, root chord, taper ratio, taper offset, two-per revolution (2/rev) harmonic control, and 2/rev blade dynamic twist) for different gross weights and flight speeds are therefore obtained by this modified procedure. In addition, the main effects and the interaction of all parameters on helicopter performance are assessed. The results of optimization in case 1 confirm that the appropriate 2/rev harmonic control and twist of the partially tapered blades improve the helicopter required power by 2.6% and lift-to-drag ratio up to about 20% at a baseline gross weight. In case 2 of optimization, tapering the blade to 60% from 0.9R with an appropriately phased 1/rev and 2/ rev twist and 2/rev harmonic control increases the rotor thrust coefficient by 23%, and the lift-to-drag-ratio by about 15%. The helicopter's gross weight is declared to influence on the thrust increment achieved by the 2/rev twist and 2/rev harmonic control. Overall, 2/rev harmonic control can be incorporated into existing helicopters by a modification of the swashplate, and control inputs can be transmitted to the rotor using a fixed outer member with a track linked to a conventional swashplate.

**Nomenclature**

$A$	Disc area	$W$	Gross weight, lb
$A_0$	Magnitude of the 0/rev twist, deg	$\alpha$	Local blade angle of attack, deg
$A_n$	Magnitude of the n/rev twist, deg	$\theta$	Blade pitch, deg
$c_0$	Root chord, ft	$\theta_0$	Collective pitch, deg

1 Assistant Professor (Corresponding Author) Email: \* prof.shahmiri@gmail.com

2 PhD. Candidate

$c_1$	Tip chord, ft	$\theta_1$	Blade twist, deg
$C_d$	Local drag coefficient	$\theta_{1c}, \theta_{1s}$	One-per-revolution lateral and longitudinal cyclic pitch, deg
$c_e$	Equivalent chord, ft	$\theta_{2c}, \theta_{2s}$	Two-per revolution lateral and longitudinal cyclic pitch, deg
$C_P$	Power coefficient, $= P / (\rho A v_t^3)$	$\rho$	Air density, slug/ft <sup>3</sup>
$C_T$	Rotor thrust coefficient, $= T / (\rho A v_t^2)$	$\sigma$	Rotor equivalent solidity, $= bc_e / \pi R$
$d_i$	Individual desirability function	$\phi_n$	Phase of n/rev twist, deg
$D$	Desirability function	$\psi$	Blade azimuth angle, deg
$k$	Central composite design points	$\Omega$	Rotor speed, rad/s
$k_c$	Center points		
$n$	Number of harmonics		
$r$	Radial distance, ft		
$R$	Blade radius, ft		
$tr$	Taper ratio, $= c_1 / c_0$		
$trst$	Taper ratio start point on the blade		
$V_\infty$	Flight speed, knots		
$v_t$	Blade tip speed, $= R\Omega$		
$w_i$	Weighting factor		

## Introduction

Higher Harmonic Control (HHC) of helicopter rotor blades has received growing attention, particularly for relieving vibratory loads and lessening noise. To this end, different actuator designs have been introduced, including high-frequency actuators, active pitch links, trailing-edge flaps, spoilers, and leading-edge elevons. The detailed reviews have been documented by [1-3]. The studies show that HHC can be extended to the concept of Higher Harmonic Stall Control (HHSC) where the principal interest is to mitigate the thrust distribution and eliminate retreating blade stall [4-7]. The HHSC differs from HHC because fundamental frequencies of HHC are  $(n - 1)\Omega$ ,  $n\Omega$ , and  $(n + 1)\Omega$  in the hub-rotating coordinate system and  $n\Omega$  in the body-fixed coordinate system. Here,  $n$  is the number of blades, and  $\Omega$  is the rotor rotational speed. In contrast to HHC, HHSC uses the usual  $2\Omega$  or second harmonic frequency, but more recent evidence also proposes the  $3\Omega$  frequency for HHSC. For example, Field [8-13] studies showed the inherent effectiveness of HHC in relieving retreating blade stall. For example, Cheng reveals that treating 2/rev inputs (2P input) improves the performance of a four-bladed

articulated rotor helicopter [11]. The goal was to examine the physical devices by which a 2/rev input alters the power required by the rotor and rotor thrust. This was achieved by simulating a helicopter in trimmed flight for different weights, flight speeds, and amplitude and phase of the two-per-revolution input. In addition, an extensive examination on the use of HHC employed through the Individual Blade Control (IBC) was performed by [14] required for stall alleviation and performance improvement. The primary function of the blade twist in improving helicopter rotor efficiency in hover and forward flight is very evident [15]. The passive twist is applied to the blade span and cannot actively change with the blade azimuth. To provide the asymmetric aerodynamic environment of the blade at the retreating and advancing sides in forward flight, a change of the spanwise and azimuthal twist distributions is required. However, actively changing blade twist has yet to be employed in helicopter rotor design. This is slightly due to challenges with the necessary equipment for the twist change and the construction of this new class of rotor blades. Yeo studied different active controls for rotor performance improvement. The one-per-revolution active blade twist had a modest influence

on the rotor performance, and the two-per-revolution harmonic control was pronounced to increase the rotor lift-to-drag ratio [16]. The benefit studies of an active twist rotor conducted by Zhang using a weak fluid-structure coupling method resulted in power reduction of about 14% [17].

Boyd used a coupled CFD/CSD (computational fluid dynamics/computational structural dynamics) approach to examine the aerodynamic and acoustic performance of an active twist rotor [18]. Kang studied several rotor morphing technologies for helicopter performance enhancement [19]. The quasi-steady blade twist resulted in 2% gains in the rotor power in forward flight. Jain reviewed three-rotor morphing concepts for performance improvement [20], particularly trailing-edge, leading-edge deflection, and active twist. The predictions by the CFD and CSD for the UH-60A rotor confirmed that the active twist degraded the power in high-speed flight by about 3.3%, and therefore no loss was achieved for the high thrust flight. The analyses of on-blade active controls conducted by Jain revealed that the 2/rev input with the 4 degrees amplitude of active twist could decrease the rotor power required by 3.3% in a high-speed forward flight [21].

The previous analyses focus on rotor performance improvements by changing the blade static twist (pre-twist) and have no attention to blade dynamic twist. However, the blade twist can be static, active, and elastic components, and all three elements can affect rotor performance. Typically, the blade twist is a sum of the static, active, and elastic twists, and it can be represented as a sum of the elements from 0/rev to  $+\infty$ /rev. Thus, we can determine the harmonic twist commands, the performance improvement, and active blade twist that can be designed for optimized performance.

Recent attention has also focused on helicopter rotor blade design optimization problems for better performance in hover and low-speed forward flight [2, 22-32]. The optimization plans are frequently conducted by combining different packages to build the optimization process. Some researchers have tried to obtain proper results using computational fluid dynamics (CFD) [33, 34]. However, severe criticism of CFD relates to its complexity and time-consuming task, especially when forward flight optimization is a problem. For instance, in hover flight, CFD evaluations are essentially confined to one design variable which is the blade twist. Consequently, the CFD is not suited for the rotorcraft preliminary design phase because of the

need for a rapid and rough estimated design. To speed up the computations in the preliminary design phase, the current work extends the first strategy without CFD and effectively describes the process improvements with particular steps.

Accordingly, this paper addresses the use of blade design planform parameters, 2/rev pitch inputs, 0-2/rev blade dynamic twist magnitudes, and corresponding phases at the different flight conditions to advance the performance of a four-bladed articulated rotor helicopter. The paper's main goal is to explore the optimum rotor blade planform through which a 2/rev input and 2/rev twist affect the power required by the rotor, lift-to-drag ratio, and, to a more limited extent, rotor thrust. This will be accomplished by the design of experiment of the experiment, simulating a helicopter in trimmed flight for various combinations of weight, flight speed, 2/rev input, and amplitude and phase of the 2/rev twist, and by desirability approach and numerical optimization technique.

### Design Optimization Process

The overall view of the design optimization process is shown in Figure 1. In the first step, the Central Composite Design (CCD) test plan is designed based on blade planform parameters, 2/rev blade dynamic twist magnitudes and phases, and 2/rev input for various flight condition parameters, and then CCD coupled with flight dynamic simulation program (FDSP) to calculate helicopter performance responses. The main score of this process is the CCD application, which is necessary to explore the optimum data, and this is rarely used in previous works, particularly in CFD optimization. Accordingly, the CCD test plan (Appendix A) is designed with 91 runs where the corresponding design space involves factorial, axial (star), and center points required for error estimation. The second step includes the validity of response models obtained from the non-linear least square method fitted to CCD data. The model validation is carried out by analysis of variance method (ANOVA) and p-value calculations. The optimization problems such as maximum rotor thrust, minimum power required, and maximum lift-to-drag ratio, are ultimately solved using the non-gradient-based optimization method [35].

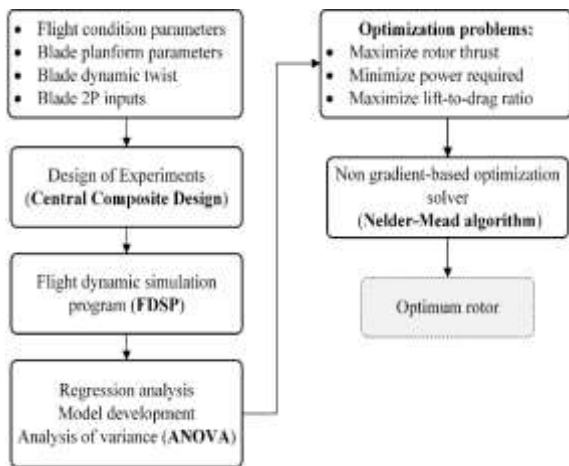
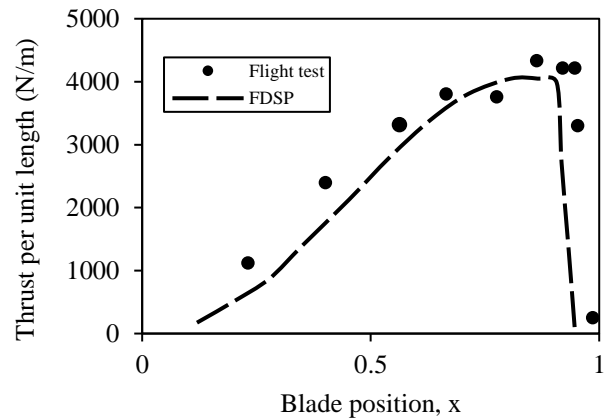


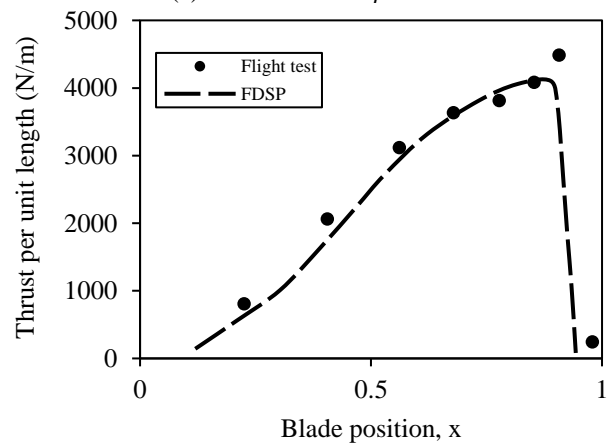
Figure 1. Rotor blade design optimization process

### Flight Dynamic Simulation Program (FDSP)

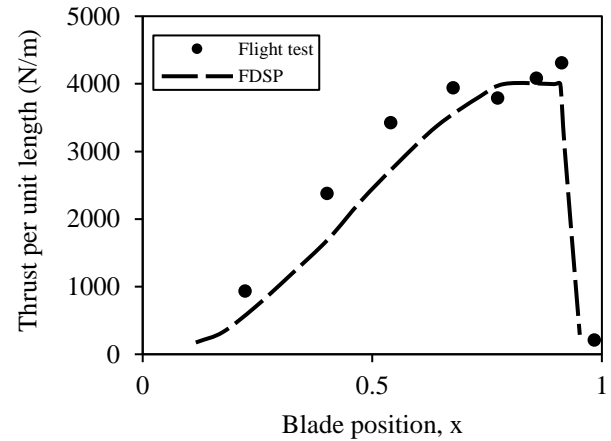
FDSP is a general flight dynamic program developed by the authors to analyze the helicopter dynamic responses [36, 37]. In this program, the rotor model is obtained by blade element theory (BET) and then numerically trimmed in three loops. The first loop is the collective pitch trim, the second loop includes the first harmonic cyclic pitch trim, and ultimately collective pitch is trimmed in the third loop. The BET and three state Pitt-Peters inflow model are applied to the rotor blade with 20 equally spaced elements [38] [39]. The Pitt-Peters model consists of uniform, sine, and cosine terms with a first harmonic azimuthal and a linear radial distribution. In the first and third loops, the value of the collective pitch is changed to achieve the required rotor thrust. However, in the second loop, the cyclic trim is obtained by calculating the initial thrust moment using cyclic pitch determined by collective trim. The process is therefore repeated when the first harmonic is removed from the thrust moment. Divergence of collective and cyclic pitch points that the blade is in the stall condition. Figure 2 and Figure 3 compare the results of FDSP against the existing flight test data for the UH-60A helicopter [40].



(a) Blade azimuth  $\psi = 0^\circ$



(b) Blade azimuth  $\psi = 90^\circ$



(c) Blade azimuth  $\psi = 180^\circ$

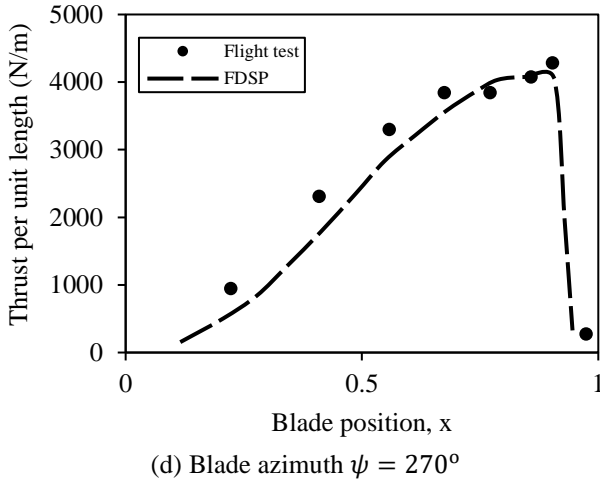


Figure 2. UH-60A thrust distribution over the blade in hover.

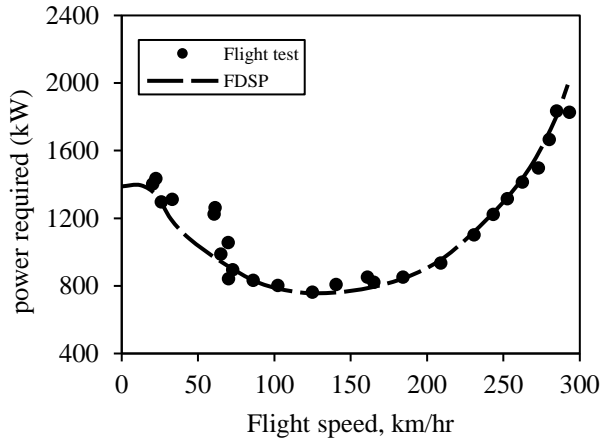


Figure 3. UH-60A power required vs. flight speed at sea level standard.

The geometric pitch angle  $\theta$  of the blade is given by [41]:

$$\theta(\psi) = \theta_0 + \theta_{1c} \cos(\psi + \Delta_{sp}) + \theta_{1s} \sin(\psi + \Delta_{sp}) + \theta_2(\psi) + \theta_{dyn}(\psi) \quad (1)$$

where  $\theta_0$  is the collective pitch,  $\theta_{1c}$  is the lateral cyclic pitch,  $\theta_{1s}$  is the longitudinal cyclic pitch,  $\Delta_{sp}$  is the swashplate phasing angle  $\Delta_{sp} = -9.7^\circ$ ,  $\theta_2(\psi)$  is the 2/rev pitch input, and  $\theta_{dyn}(\psi)$  is the 2/rev blade twist, respectively, defined as:

$$\theta_2(\psi) = \theta_{2c} \cos(2\psi + \Delta_{sp}) + \theta_{2s} \sin(2\psi + \Delta_{sp}) \quad (2)$$

and

$$\theta_{dyn}(\psi) = \frac{r}{R} [A_0 + A_n \cos(n\psi + \Delta_{sp} - \phi_n)] \quad (3)$$

where  $\theta_{2c}$  and  $\theta_{2s}$  in Eq. (2) denotes 2P cosine and 2P sine inputs, respectively. In Eq. (3),  $A_0$  presents the magnitude of the 0/rev twist, and  $(A_n, \phi_n)$  are the

magnitude and corresponding phase of the n/rev twist.

Here, the lateral and longitudinal cyclic pitches are determined by FDSP using the first harmonic trim routine, and the 2P sine and cosine inputs, Eq. (2), are user-defined approximations. In the current work, the 2P sine input in Eq. (2) was assumed to be zero because 2P sine values increase the blade stall region at the retreating sides of the rotor disc. It should be noted that effective results were also obtained by 3P inputs, particularly in experimental analyses. Still, these terms were also set to zero because, in most cases, the trim solutions were not available by FDSP.

### Design Parameters

The different rotor blade design parameters, root chord, taper ratio, taper point on the blade, 2P cosine input, magnitudes, and phases of the blade dynamic twist within flight speed and gross weight were all chosen for our optimization problems (Table 1). The intervals were specified based on the power required less than the power available and the equivalent blade loading bounded to blade stall value. The upper limit of the gross weight was required to examine directly the impacts of the above-mentioned parameters on the maximum rotor thrust. In this research, the maximum gross weight was determined based on the maximum trimmable weight of the UH-60A helicopter at the upper and lower level of forward flight speed. Therefore, for each level of speed, the weight was increased in 500-lb increments from 17,665 lb (baseline), till the helicopter could no longer be trimmed. Overall, 17,500 and 22,000 lb values were employed for the whole study.

In this work, the blade was supposed to be rectangular up to the given taper point and then tapered to the tip from 0.6 to 0.9R. The taper ratio is defined as  $c_1/c_0$ , where  $c_1$  is the tip chord and  $c_0$  denotes the root chord. The blade taper ratio was changed from 0.4 to 0.6 at which the values of equivalent blade loadings were all less than 0.14. In this case, the rotor mean lift coefficient was lower than the maximum lift coefficient of SC1095R8 airfoil, and thus the rotor blade stall was sufficiently avoided. The magnitudes of blade dynamic twist  $(A_1, A_2)$  were defined between zero to  $1^\circ$  and their corresponding phases  $(\phi_1, \phi_2)$  were considered in the range of zero to  $360^\circ$ . The 0/rev or static twist was changed between  $-20^\circ$  to  $-10^\circ$ . To modify the rotor blade stall pattern, the 2P cosine input was

therefore increased from 1° to 2°. This range was used and ensured that the trim conditions for the whole platform are available.

**Table 1.** Rotor blade design parameters.

Design parameters	Units	Coded value	Lower value	Baseline	Upper value
Flight speed, $V_\infty$	knots	A	80	80	140
Gross weight, $W$	lbs	B	17,500	17,665	22,000
Root chord, $c_0$	ft	C	1.5	1.73	3.5
Taper ratio, $tr$		D	0.4	1	0.6
Taper offset, $trst$		E	0.6R	0	0.9R
0/rev twist, $A_0$	deg	F	-20	-18	-10
1/rev twist, $A_1$	deg	G	0	0	1
2/rev twist, $A_2$	deg	H	0	0	1
1 <sup>st</sup> twist phase, $\phi_1$	deg	J	0	0	360
2 <sup>nd</sup> twist phase, $\phi_2$	deg	K	0	0	360
2/rev cosine input, $2P$	deg	M	1	0	2

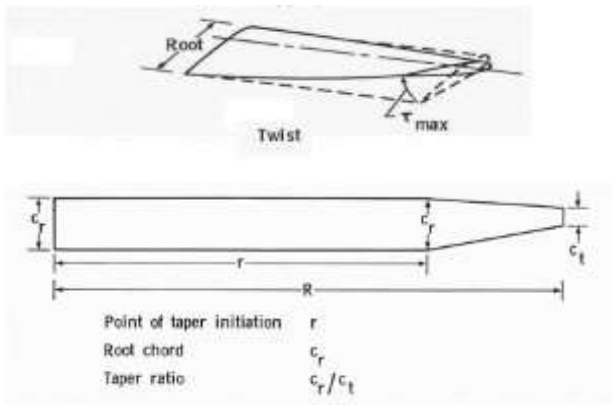


**Figure 4.** Blade Geometry Parameters.

**Data Sampling and Modeling**

Experimental design is required for a precise performance evaluation and is conducted before data gathering in this paper. Audet and Tribes showed that CCD is better designed than Box–Behnken, Dohert, and three-level factorial methods because the axial points make it rotatable and 5-level design in CCD points is evident [42] [43]. Consequently, of the different design methods, in the first step, CCD with  $2^k + 2k + k_c$  points were chosen for the data collection with  $k = 11$  and a center point  $k_c = 1$  but the total number of runs was 2071. We received a great challenge to continue with these lots of experiments. To avoid this, the “Min-Run Res V” was ultimately used as a reduced form of rotatable CCD and the number of runs was significantly decreased to 91 samples (Appendix A). From the data given in Appendix A, the normalized

performance models are derived and shown in Figure 5 to Figure 7.

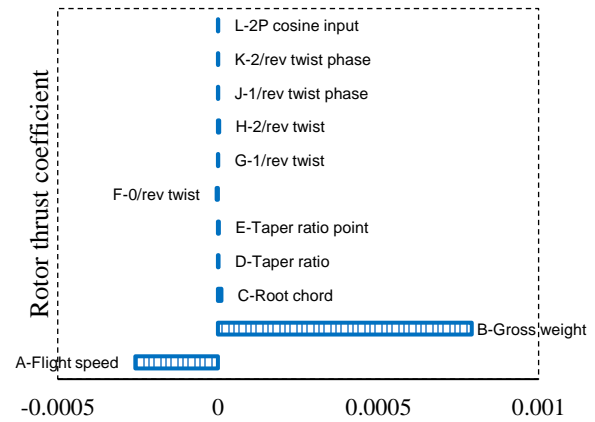


**Figure 5.** Rotor thrust model coefficients of UH-60A helicopter in standard sea-level.

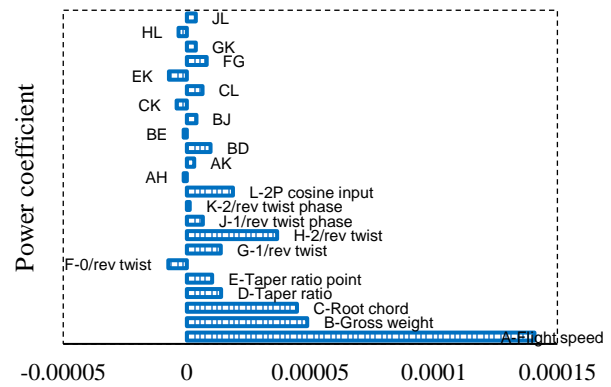


**Figure 6.** Power model coefficients of UH-60A helicopter in standard sea-level.

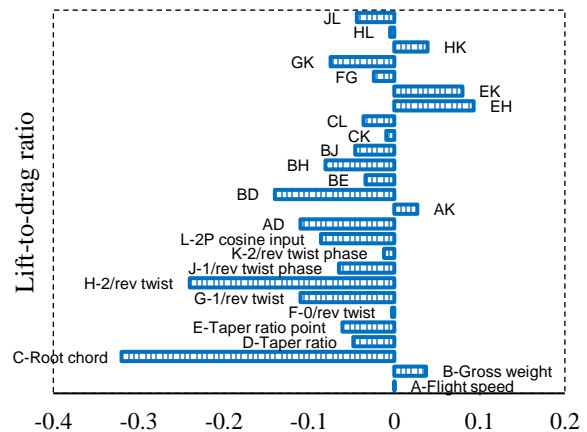


**Figure 7.** Lift-to-drag ratio model coefficients of UH-60A helicopter in standard sea-level.

As seen in the figures, these normalized (coded) forms of parameters are adequate to compare the main effects and interactions on each response. The analysis of variance (ANOVA) of the developed models is shown in Table 2 where the models are significant in 95% confidence level (p-value < 0.05).

**Table 2.** Results of ANOVA for the developed models

Model	Sum of square	Mean square	p-value
Thrust coefficient	2.411E-005	8.930E-007	< 0.0001
Power coefficient	4.138E-006	1.118E-007	< 0.0001
Lift-to-drag ratio	18.82	0.51	<0.0001

The most critical parameters, affecting the main rotor thrust coefficient are given in **Error! Reference source not found.** In this figure, the steep slopes confirm the dominant effect, and zero slope lines show the least impact affected rotor thrust coefficient in forward flight. Note that these lines are achieved by changing a selected parameter in a given range [-1 1] while the other factors are constant. Accordingly, the notable variations in the thrust coefficient through changes in gross weight and forward flight speed are evident. Contrary to expectations, other parameters (i.e., blade planforms, 0-2/rev blade dynamic twist, and 2P

cosine input) do not affect the rotor thrust coefficient in medium to high-speed forward flight. This result is also confirmed by the response surfaces given in Figure 9.

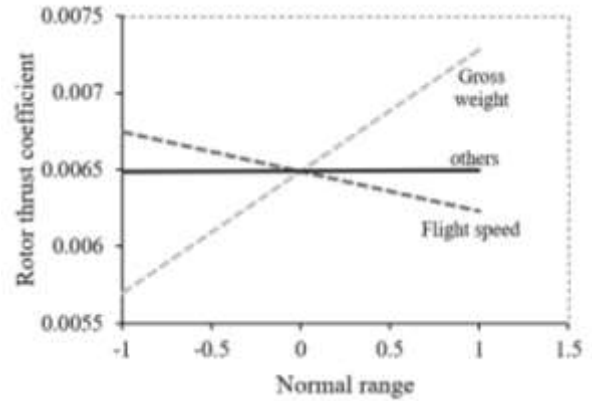
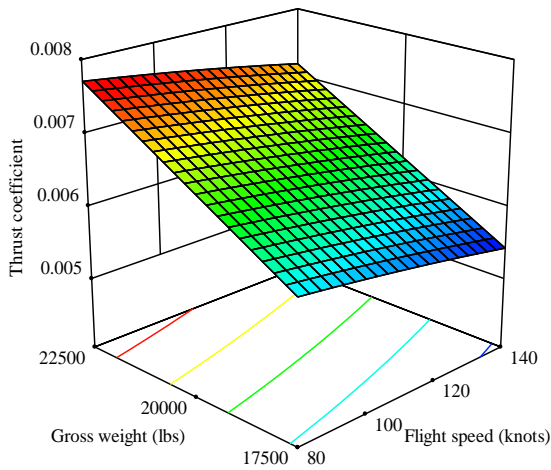
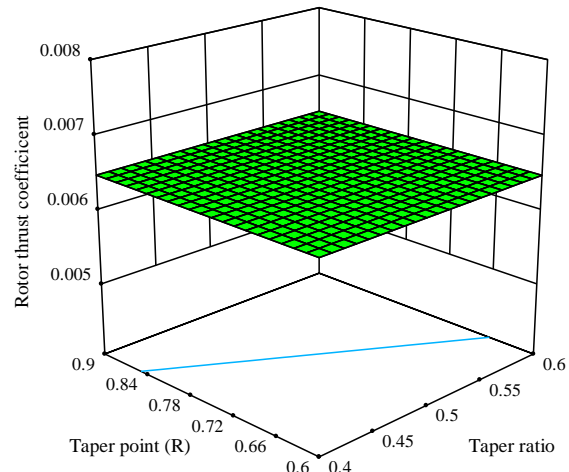


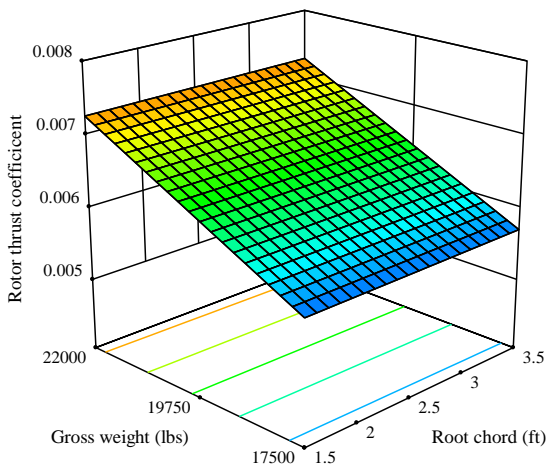
**Figure 8.** Sensitivity of rotor thrust coefficient of UH-60A helicopter to rotor blade design parameters.



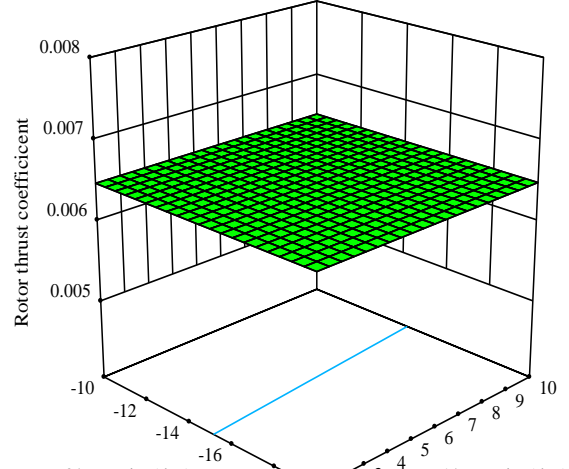
a)



b)



c)



d)

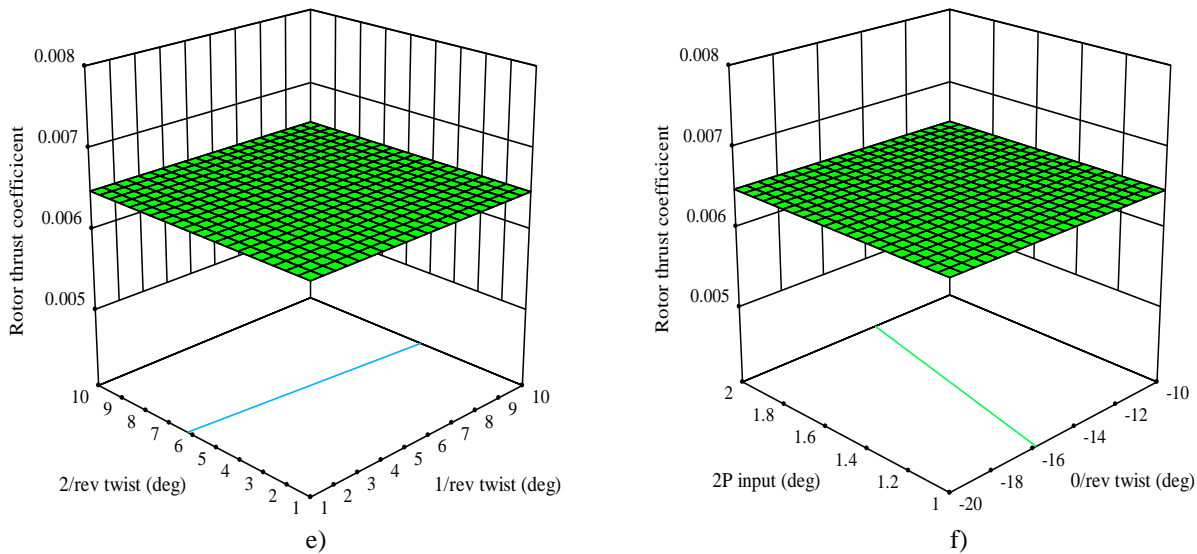


Figure 9. Representation of UH-60A rotor thrust variations versus blade design parameters.

The response surfaces in Figure 9(a) are in line with the results shown in **Error! Reference source not found.**. The dominant effect of gross weight on rotor thrust coefficient is evident for the UH-60A helicopter in forward flight. Also, flight speed is the second significant factor affecting the rotor thrust. Surprisingly, the rotor thrust coefficient is insensitive to the other blade planform parameters (see Figure 9(b) to Figure 9 (f)). The flat response surfaces confirm the insensitivity of the rotor thrust coefficient to the root chord, taper ratio, taper point on the blade, 2/rev blade dynamic twist, and 2P cosine input. Overall, the importance of the helicopter's gross weight on rotor thrust is emphasized too much in this section.

The main factors, influencing the helicopter power coefficient, are illustrated in Figure 10. As shown in Figure 10, among all chosen design parameters, flight speed, gross weight, and blade root chord on power coefficient are respectively significant. However, very slight variations of power required are taken by the 0-2/rev blade twists, 2P cosine input, and taper ratio. Surprisingly, other parameters do not have tremendous effects on the amount of helicopter power required, and thus their slope of lines is approximately close to zero.

Unlike other research carried out in this area, we did not find a negative effect of 2P cosine input on the

power required of the UH-60A. The main reason for this is notable interactions between 2P cosine input with blade root chord, 1/rev twist phase, and 2/rev blade twist that have not been modeled in the previous literature. This result is also further proved by the response surfaces illustrated in Figure 11.

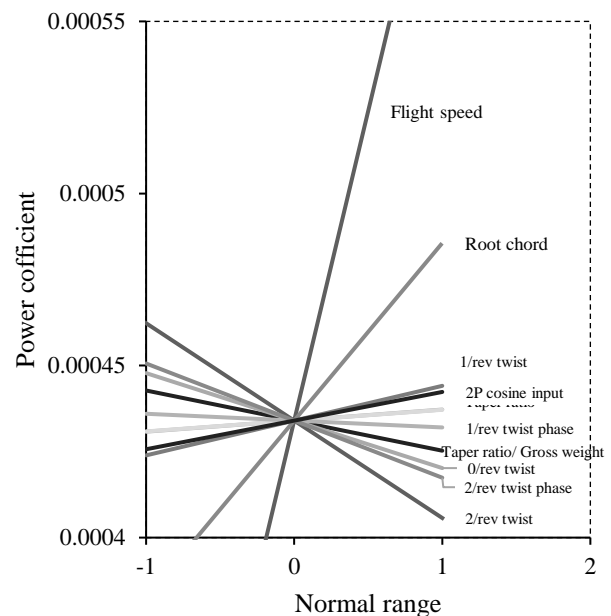
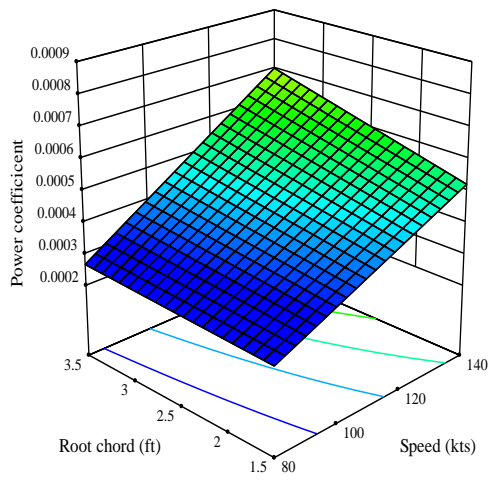
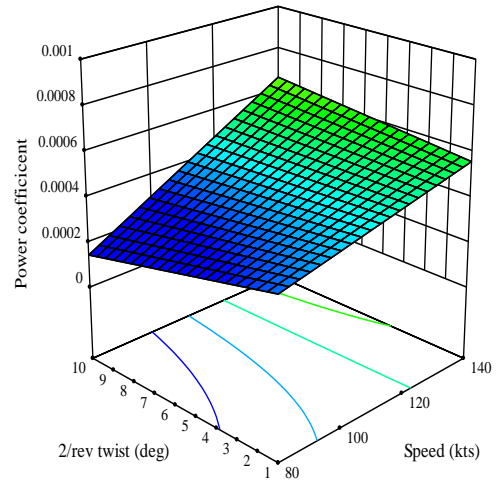


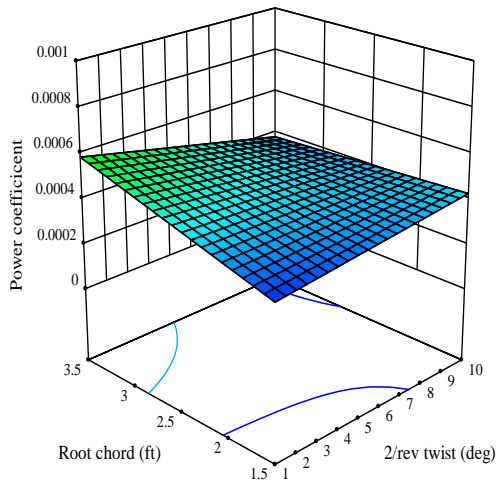
Figure 10. Sensitivity of rotor power coefficient of UH-60A helicopter to rotor blade design parameters.



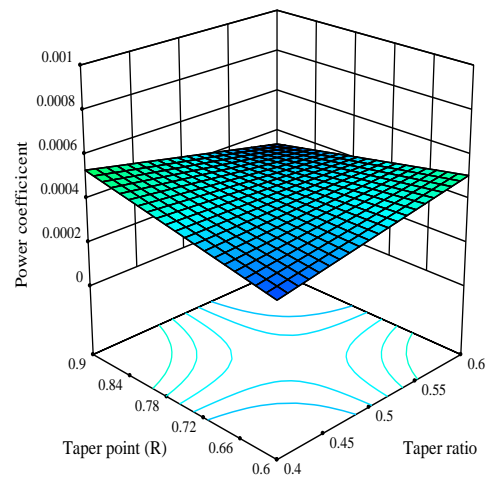
a)



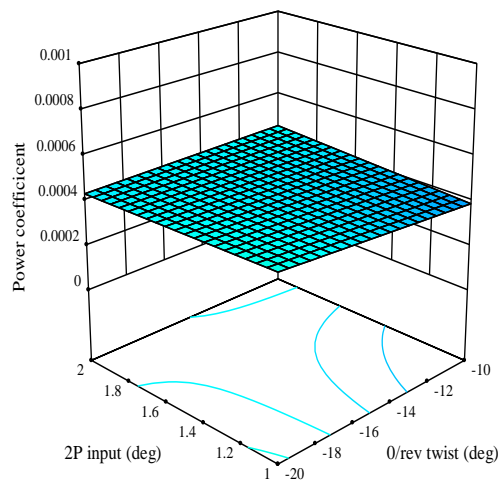
b)



c)



d)



e)

**Figure 11.** Representation of UH-60A rotor power variations versus blade design parameters

The effects of forward flight speed, blade root chord, gross weight, and 2/rev blade twist on helicopter power coefficient are presented in Figure 11(a) to 11(e). The notable increase of power coefficient with increasing helicopter flight speed is obvious in Figure 11(a). The main reason for this is the increase of parasite power which is proportional to the cube of flight speed. The increase of the power coefficient with the blade root chord is attributed to the equivalent rotor solidity that is a prime cause for the growth of the rotor profile power in forward flight. The obtained results indicate that the taper ratio and taper starting point on the blade compared with forward flight speed, blade root chord, and 2/rev blade twist are insignificant factors affecting the power required in forward flight.

The effects of forward flight speed, blade root chord, gross weight, and 2/rev blade twist on helicopter power coefficient are presented in Figure 11 (a) to 11 (e). The notable increase of power coefficient with increasing helicopter flight speed is obvious in Figure 11(a). The main reason for this is the increase of parasite power which is proportional to the cube of flight speed. The increase of the power coefficient with the blade root chord is attributed to the equivalent rotor solidity that is a prime cause for the growth of the rotor profile power in forward flight. The obtained results indicate that the taper ratio and taper starting point on the blade compared with forward flight speed, blade root chord, and 2/rev blade twist are Figure 11 (b) compares the effects of 2/rev blade twist and forward flight speed and Figure 11(c) highlights the role of the blade root chord and 2/rev blade twist on UH-60A helicopter power required. A significant difference between the flight speed and the 2/rev blade twist on the power coefficient is realized in Figure 11(b). Although not shown in the paper, a one-factor plot proves that the flight speed presents greater effects on helicopter power coefficient than the 2/rev blade twist.

The results in Figure 11(c) confirm that, with decreasing blade root chord and 2/rev twist, the power coefficient is partially saved in forward flight. Also, the variations of power to the root chord are more significant than the 2/rev twist and this result approves the previous results given in Figure 10.

Figure 11 (d) shows that tapering the blade from 0.6R leads to helicopter power loss, which contrasts with the tapered tip starting point of 0.9R. This figure also reveals that the helicopter power coefficient is independent of the blade taper ratio

when the taper starting point is about 0.75R. Accordingly, the minimum power coefficient is obtained by either a taper starting point of 0.6R at the lowest taper ratio or a taper starting point of 0.9R at the highest taper ratio.

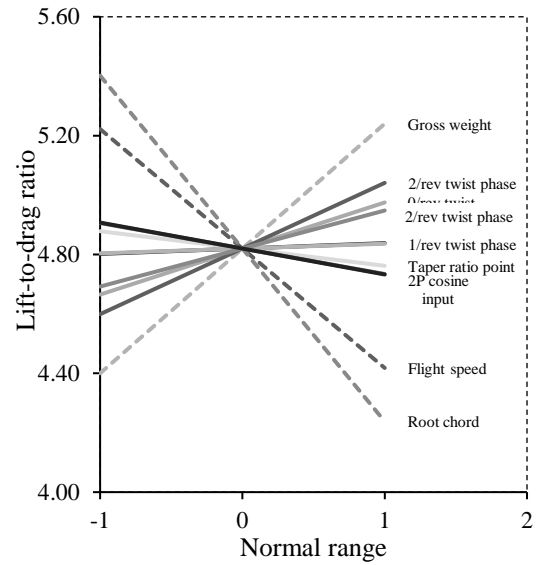
Figure 11(e) presents the effects of the blade static twist (0/rev twist) and 2P cosine input on the power required of the UH-60A helicopter. As can be seen in Figure 11(e), the 2P input and 0/rev twist do not significantly affect the power coefficient in forward flight. Although not presented, the one-factor plot highlights a slight increase of power required obtained by increasing the 2P cosine input. This result contrasts with the results published by [11] because, in the current paper, the interaction of 2P cosine input, 0/rev, and 2/rev twist parameters on the power coefficient model is effectively considered. Thus, the 2P cosine input significantly increases the helicopter power coefficient in forward flight.

Figure 12 exhibits the results of forward flight efficiency to blade design planform parameters and confirms that the most significant parameter is the blade root chord. The reason for this is due to an increase in rotor solidity that leads to a high profile drag and a low blade loading resulting in the reduction of the rotor mean lift coefficient and a higher lift-to-drag ratio. Figure 12 also compares the impacts of flight speed and gross weight on aerodynamic efficiency, which are approximately the same. This figure shows the positive influences of flight speed and the adverse effects of gross weight. In addition, the 2/rev twist is considered the main effect on the lift-to-drag ratio. However, due to the interaction effects between the 2/rev and 0/rev twist, it is a bit difficult to interpret the outcomes of the 2/rev twist and its effectiveness on the lift-to-drag response.

Moreover, the interaction between the 2/rev twist and 2P cosine input on the lift-to-drag ratio is significant. Although not shown, the interaction plot points that at 0/rev twist of  $-13^\circ$  and 2P cosine input of  $1.6^\circ$ , the lift-to-drag ratio is independent of the 2/rev twist. Furthermore, the result also reveals that lift-to-drag strongly depends on the interaction between 2/rev and 1/rev twists. Interestingly, at a maximum 1/rev of  $10^\circ$ , the lift-to-drag ratio is free of the 2/rev twist, while a 2/rev twist is proposed as a main effect for the lift-to-drag response.

As shown in Figure 12, the negative effect of 2P cosine input on the lift-to-drag ratio is obvious. The main cause for this is increased rotor profile power (drag) when 2P cosine input with zero phase is

applied. The increase in rotor profile power is proved by tracing the peaks in the local torque in the outer portions of the front and the rear of the disk. What is to be said is that the profile torque peaks are primarily caused by increases in drag coefficient, where its increments are related to the combined effect of angle of attack and Mach number. For example, On the front and the rear of the rotor disc, the 2P cosine input is maximum, and the drag coefficient increases compared with the baseline case  $2P = 0^\circ$ . The opposite occurs on the right and left sides of the disk, where the 2P cosine input is minimum.



**Figure 12.** Sensitivity of lift-to-drag ratio of UH-60A helicopter to rotor blade design parameters.

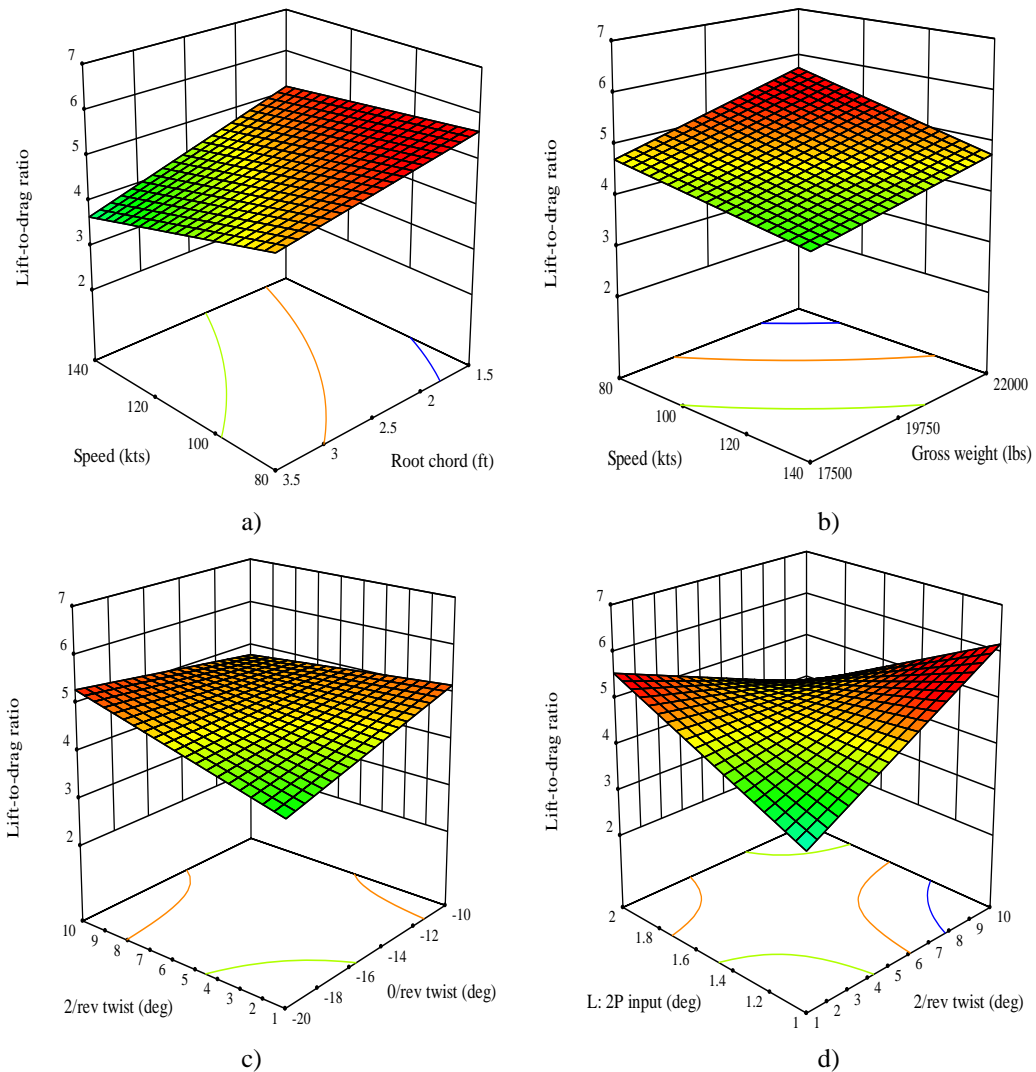


**Figure 13.** Sensitivity of lift-to-drag ratio of UH-60A helicopter to rotor blade design parameters.

The effects of the root chord and forward flight variations on lift-to-drag response are shown in Figure 13(a). The blade root chord significantly influences the lift-to-drag ratio in forward flight among all selected parameters. The possible explanation for this is that the greater root chord leads to the larger equivalent rotor solidity, and thus the greater rotor profile power is achieved. This plot confirms that with the minimum root chord of 1.5 ft and minimum flight speed of 80 knots, the maximum aerodynamic efficiency is 5.63.

Figure 13(b) shows forward flight speed and gross weight effects on lift-to-drag variations in medium to high-speed forward flight. For the 22,000 lb case, the maximum lift-to-drag ratio of 5.73 is achieved at 80 knots while compared to the speed of 140 knots, its value is 17% higher.

Figure 13(c) also highlights the effects of the 2/rev and 0/rev twists on the efficiency of the UH-60A helicopter in forward flight. The results show that for the maximum values of 2/rev and 0/rev twist, the maximum lift-to-drag ratio of 5.29 is achieved. Interestingly, at a 0/rev twist of 12.5°, the amount of lift-to-drag ratio does not depend on 2/rev twist changes. For 0/rev twist less than 12.5°, the maximum lift-to-drag ratio is assessed at a maximum value of 2/rev twist and values greater than 12.5°; the maximum lift-to-drag ratio is 5.16, representing a reduction of 2.6%.

The interaction between the 2/rev twist and 2P cosine input variables is obvious in Figure 13(d). Here, the maximum lift-to-drag ratio of 6.18 is achieved by a maximum 2/rev twist at minimum 2P cosine input. It should be noted that at a 2/rev twist of about 5°, the magnitude of lift-to-drag is independent of the 2P cosine input. Using a 2/rev twist less than 5 degrees for a maximum of 2P cosine input, the greatest lift-to-drag is about 5.56. However, at a 2/rev twist higher than 5°, the lift-to-drag ratio 6.18 is achieved for a minimum of 2P cosine input. As expected, the effects of interactions do not allow the main effects to play a significant role in lift-to-drag ratio changes. Overall, the impacts of 2P cosine input compared to 2/rev twist are relatively severe but in comparison with other variables such as root chord and speed is very modest and negligible.

## Results

The desirability function approach is suited for resolving the conflict among the multiple responses based on a dimension reduction strategy. Therefore,

the desirability method was employed for two optimization problems defined in Table 3 of the different optimization approaches. To this end, the optimum blade planform for the UH-60A helicopter in forward flight is sought based on the combination of maximum rotor thrust coefficient, minimum power required coefficient, and maximum lift-to-drag ratio listed in **Error! Reference source not found.** In case 1, the goal is to determine the maximum  $L/D$  and minimum  $C_p$  at a baseline gross weight of 17,665 lb. Case 2 includes maximum  $L/D$ , minimum  $C_p$ , and maximum  $C_T$  in the range of 17,500 lb to 22,000 lb.

**Table 3.** Definition of design optimization problems

Case	Design goal
1	Maximize $L/D$ and Minimize $C_p$
2	Maximize $L/D$ , Minimize $C_p$ , and Maximize $C_T$

Here, the problems were reduced to desirability (objective) function as [23];

$$\text{Maximize } D = \sqrt[3]{d_1 d_2 d_3} \quad (4)$$

where the individual desirability ( $d_i$ ) corresponding to each response is:

$$d_1 = \begin{cases} 0 & C_T < C_T^{\min} \\ \left[ \frac{C_T - C_T^{\min}}{C_T^{\max} - C_T^{\min}} \right]^{w_1} & C_T^{\min} \leq C_T \leq C_T^{\max} \\ 1 & C_T > C_T^{\max} \end{cases}$$

$$d_2 = \begin{cases} 1 & C_p < C_p^{\min} \\ \left[ \frac{C_p^{\min} - C_p}{C_p^{\max} - C_p^{\min}} \right]^{w_2} & C_p^{\min} \leq C_p \leq C_p^{\max} \\ 0 & C_p > C_p^{\max} \end{cases}$$

$$d_3 = \begin{cases} 0 & L/D < L/D^{\min} \\ \left[ \frac{L/D - L/D^{\min}}{L/D^{\max} - L/D^{\min}} \right]^{w_3} & L/D^{\min} \leq L/D \leq L/D^{\max} \\ 1 & L/D > L/D^{\max} \end{cases}$$

In the above-mentioned equations,  $w_i$  the weighting factor was set to 10 because the authors were interested in the maximum emphasis on the aim of optimization. Although not shown, this paper selected this weighting factor based on

supplementary analysis on a different combination of weighting factors.

The results of optimization problems compared with the baseline case are summarized in Table 4. The maximum lift-to-drag ratio of 5.43 and minimum power coefficient of  $3.02 \times 10^{-4}$  at a baseline gross weight of 17,665 lb is evident in case 1. In this case, tapering the tip to 57% starting from 0.787R, blade dynamic twist amplitudes of  $A_1 = 1.15^\circ$  and  $A_2 = 2.9^\circ$  and with the corresponding phases of  $\phi_1 = 207^\circ$  and  $\phi_2 = 203^\circ$  and also 2P cosine input of  $1.07^\circ$  resulted in an improvement in power required and lift-to-drag ratio. These gains in forward flight efficiency are attributed to small solidity and smaller profile power obtained by tapering. What is to be said is that the peak of the lift-to-drag ratio is raised from baseline 4.51 to 5.34, a 20.4% gain. This value corresponds to a 2.6% gain for power coefficient of case 1.

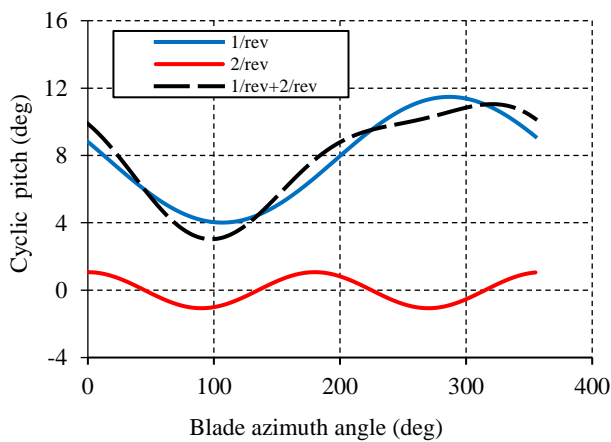
In case 2, the power coefficient is reduced by about 32% and the static twist increases from  $-18^\circ$  to  $-19.7^\circ$  to compensate for the increment of lift due to smaller equivalent rotor solidity (about 11%). It should be noted that the improvement in forward flight is also due to 2P cosine input of  $1.0^\circ$  and the proper choice of amplitudes and phases for the dynamic twist (**Error! Reference source not found.**). The above results are concerned with the flight condition at which the gross weight is 22,000 lb. However, in this case where the gross weight is larger than baseline weight the rotor thrust coefficient is increased by 23%. Moreover, the optimum blade planform leads to uniform inflow over the rotor disc

from 0.9R to the tip, and thus the reduction in induced power for the new tapered blade is obvious.

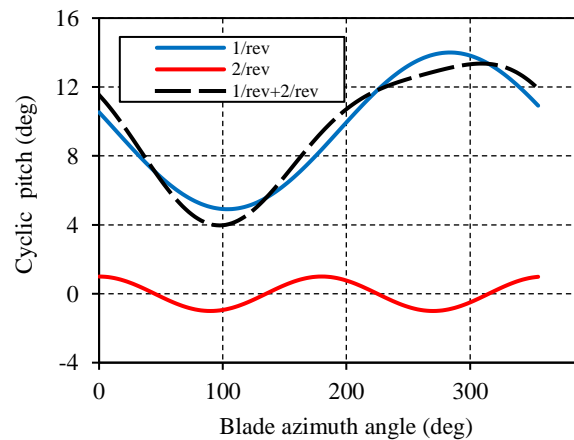
**Table 5.** Optimum solution of multi-response optimization problems.

Design parameter	Case 1	Case 2	Baseline
Flight speed, knots	93	94	80
Gross weight, lbs	17,665	22,000	17,665
Root chord, ft	1.53	1.5	1.73
Taper ratio	0.43	0.401	1
Taper offset	0.787	0.9	0
0/rev twist, deg	-16	-19.7	-18
1/rev twist, deg	1.15	1.03	0
2/rev twist, deg	2.9	1	0
1 <sup>st</sup> harmonic phase, deg	207	355	0
2 <sup>nd</sup> harmonic phase, deg	203	173	0
2P cosine input, deg	1.07	1	0
Thrust coefficient	0.006	0.00741	0.006
Power coefficient	0.000302	0.00041	0.00031
Lift-to-drag ratio	5.43	5.21	4.51

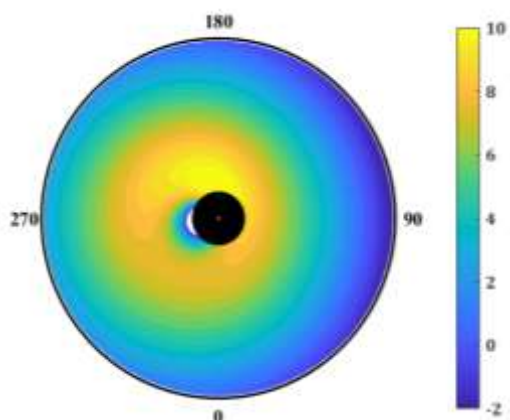
As mentioned earlier, the main reason for using 2P cosine input is to improve the aerodynamic efficiency of the rotor by shifting and changing the rotor stall region. Accordingly, **Error! Reference source not found.** and Figure 14 were chosen because the stall patterns are directly related to the angle of attack distribution.



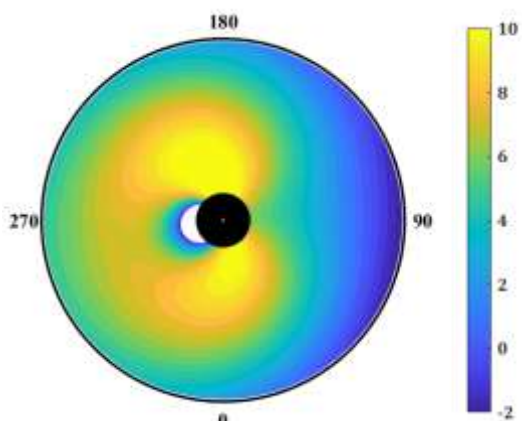
a) Case 1



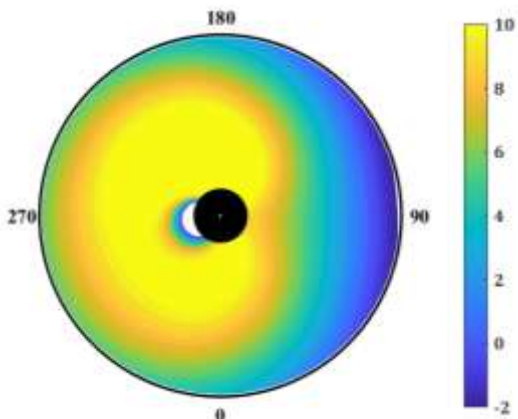
b) Case 2



a) Baseline

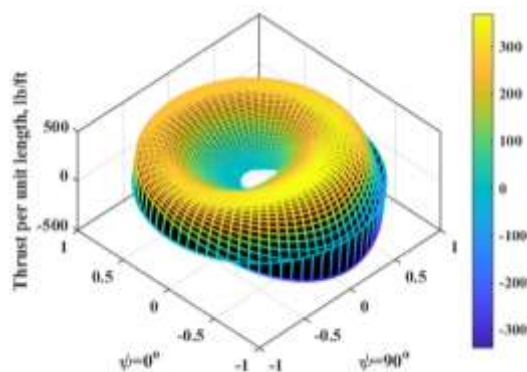


b) Case 1

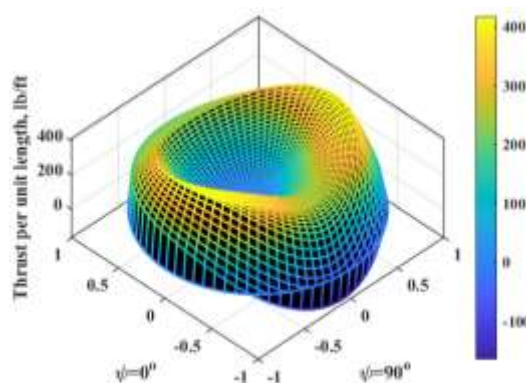


c) Case 2

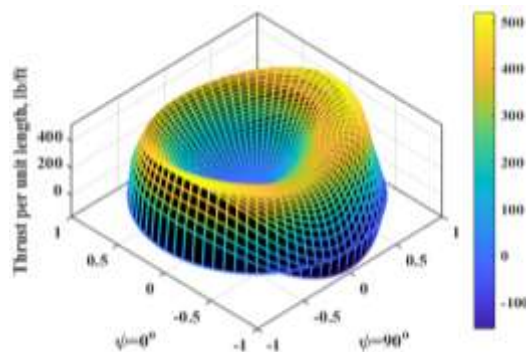
**Figure 14.** Two-per revolution input and dynamic twist effects on angle of attack distribution. Three-dimensional thrust distribution graphs were drawn to further verify the effects of the higher harmonic inputs and blade dynamic twist. The plots are compared to baseline thrust distributions in Figure 15(a) to 16(c).



a) Baseline



a) Case 1



b) Case 2

**Figure 15.** Baseline 1/rev thrust distribution (top) compared to 2/rev and blade dynamic twist thrust distribution (case 1 and case 2).

Figure 15(b) and 16(c) show the effects of 2P input on the rotor angle of attack distribution. These figures highlight that the UH-60A helicopter flies on the fore and aft sections of the rotor disc and therefore does not rely on the lift of the retreating and advancing side of the rotor. Consequently, the rotor is no longer attempting to provide propulsive and thrust force from the retreating and advancing

sides. As a result, this is interpreted as an ability to gain forward velocity.

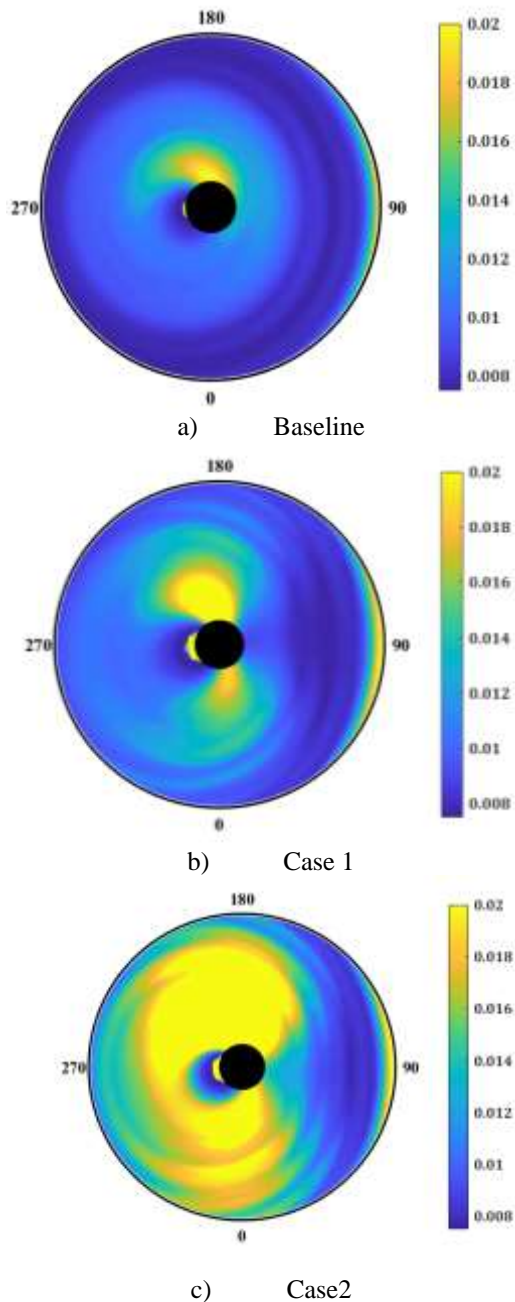


**Figure 16.** Baseline 1/rev drag distribution (left) compared to 2/rev and dynamic twist drag distribution.

The rotor distributions of local drag coefficients  $C_d$  are also shown in the Figure 16(a) to 17(c). They indicate that the profile power peaks are primarily caused by increases in  $C_d$  in the front and aft section of rotor disc.

## Conclusions

A systematic evaluation was carried out to determine the optimum rotor blade planform and

performance improvements using blade dynamic twist and higher harmonic control inputs. The central composite design was used for data exploring using the flight dynamic simulation program previously validated against flight test data. The predictions of the optimum power required and lift-to-drag ratio by desirability approach and numerical optimization method are performed and confirms that this work is a step towards advancing the rotor blade design optimization process and the main findings are:

- 1) Partially tapered blades, blade dynamic twist, and higher harmonic controls can be used to reduce helicopter power and improve flight efficiency in medium to high-speed forward flight.
- 2) The interaction of rotor design parameters can be a severe challenge to identify the main effects influencing helicopter performance.
- 3) In case 1, tapering the tip to 57% initiating from 0.78R with a properly phased 1/rev and 2/ rev twist and 2/rev cyclic pitch input reduces the power coefficient by 2.6% and significantly enhances the lift-to-drag-ratio by about 20% relative to the baseline case. This benefit can be justified by smaller equivalent rotor solidity and the lower profile power provided by the optimum blade planform.
- 4) The power reductions by the higher harmonic blade dynamic twist and 2/rev cyclic pitch input are substantially small. The zero harmonic twist presents a better result than the higher harmonic twist. The 2/rev cyclic pitch input alleviates the retreating blade stall by moving the stall region to the fore section of the rotor disc and a 16% increase in speed of maximum lift-to-drag ratio is evident.
- 5) In case 2, tapering the blade to 60% from 0.9R with an appropriately phased 1/rev and 2/ rev twist and 2/rev lateral cyclic pitch input increases the rotor thrust coefficient by 23%, and the lift-to-drag-ratio by about 15%. In this case, the increment of the power loss to baseline power can be justified by the addition of local drag coefficient of rotor blade at gross weight of 22,000 lb. The helicopter gross weight can have a pronounced effect on the power reductions achieved using the dynamic blade twist and harmonic controls.

## Conflict of interest statement

The authors declare no conflict of interest to this work.

## Reference:

- [1] Friedmann, P.P. and T.A. Millott, *Vibration reduction in rotorcraft using active control—a comparison of various approaches*. Journal of Guidance, Control, and Dynamics, 1995. **18**(4): p. 664-673.
- [2] Glaz, B., et al., *Multiple-surrogate approach to helicopter rotor blade vibration reduction*. AIAA journal, 2009. **47**(1): p. 271-282.
- [3] Hammond, C.E., *Higher Harmonic Control: A Historical Perspective*. Journal of the American Helicopter Society, 2021. **66**(2): p. 1-14.
- [4] Stewart, W., *Second harmonic control on the helicopter rotor*. 1952.
- [5] Payne, P., *Higher harmonic rotor control: the possibilities of third and higher harmonic feathering for delaying the stall limit in helicopters*. Aircraft Engineering and Aerospace Technology, 1958.
- [6] Arcidiacono, P.J., *Theoretical performance of helicopters having second and higher harmonic feathering control*. Journal of the American Helicopter Society, 1961. **6**(2): p. 8-19.
- [7] Ham, N.D., *Helicopter individual-blade-control research at MIT 1977-1985*. 1986.
- [8] Cheng, R.P., C.R. Theodore, and R. Celi, *Effects of two/rev higher harmonic control on rotor performance*. Journal of the American Helicopter Society, 2003. **48**(1): p. 18-27.
- [9] Giovanetti, E.B. and K.C. Hall, *Optimum design of compound helicopters that use higher harmonic control*. Journal of Aircraft, 2015. **52**(5): p. 1444-1453.
- [10] Hall, K.C. and E.B. Giovanetti, *Minimum Power Requirements and Optimal Rotor Design for Conventional and Compound Helicopters Using Higher Harmonic Blade Root Control*. 2016, Duke University Durham United States.
- [11] Cheng, R.P. and R. Celi, *Optimum two-per-revolution inputs for improved rotor performance*. Journal of Aircraft, 2005. **42**(6): p. 1409-1417.
- [12] Norman, T.R., et al. *Full-scale wind tunnel test of a UH-60 individual blade control system for performance improvement and vibration, loads, and noise control*. in *American Helicopter Society 65th Annual Forum, Grapevine, TX*. 2009.
- [13] Cheng, R., C. Theodore, and R. Celi. *Effects of higher harmonic control on rotor performance*. in *ANNUAL FORUM PROCEEDINGS-AMERICAN HELICOPTER SOCIETY*. 2000. AMERICAN HELICOPTER SOCIETY, INC.
- [14] Park, J.-S., et al., *Vibration and performance analyses using individual blade pitch controls for lift-offset rotors*. International Journal of Aerospace Engineering, 2019. **2019**.
- [15] Gessow, A., *Flight Investigation of Effects of Rotor-blade Twist on Helicopter Performance in the High-speed and Vertical-autorotative-descent Conditions*. 1948: National Advisory Committee for Aeronautics.
- [16] Yeo, H., *Assessment of active controls for rotor performance enhancement*. Journal of the American Helicopter Society, 2008. **53**(2): p. 152-163.
- [17] Zhang, Q., F. Hoffmann, and B.G. van der Wall, *Benefit studies for rotor with active twist control using weak fluid-structure coupling*. 2009.
- [18] Boyd Jr, D.D. *Initial aerodynamic and acoustic study of an active twist rotor using a loosely coupled CFD/CSD method*. in *35th European Rotorcraft Forum, Hamburg, Germany*. 2009.
- [19] Kang, H., H. Saberi, and F. Gandhi, *Dynamic blade shape for improved helicopter rotor performance*. Journal of the American Helicopter Society, 2010. **55**(3): p. 32008-32008.
- [20] Jain, R., H. Yeo, and I. Chopra, *Computational fluid dynamics—computational structural dynamics analysis of active control of helicopter rotor for performance improvement*. Journal of the American Helicopter Society, 2010. **55**(4): p. 42004-42004.
- [21] Jain, R., H. Yeo, and I. Chopra, *Examination of rotor loads due to on-blade active controls for performance enhancement*. Journal of aircraft, 2010. **47**(6): p. 2049-2066.
- [22] Walsh, J.L., G.J. Bingham, and M.F. Riley, *Optimization methods applied to the aerodynamic design of helicopter rotor blades*. Journal of the American Helicopter Society, 1987. **32**(4): p. 39-44.
- [23] Giguere, P. and M. Selig, S, *Design of a tapered and twisted blade for the NREL combined experiment rotor*. 1999, National Renewable Energy Lab., Golden, CO (US).
- [24] Le Pape, A. and P. Beaumier, *Numerical optimization of helicopter rotor aerodynamic performance in hover*. Aerospace Science and Technology, 2005. **9**(3): p. 191-201.
- [25] Sun, H. and S. Lee, *Response surface approach to aerodynamic optimization design of helicopter rotor blade*. International journal for numerical methods in engineering, 2005. **64**(1): p. 125-142.
- [26] Chae, S., et al., *Helicopter rotor shape optimization for the improvement of aeroacoustic performance in hover*. Journal of Aircraft, 2010. **47**(5): p. 1770-1783.
- [27] Darwish, S., et al. *Aerodynamic shape optimization of helicopter rotor blades in hover using genetic algorithm and adjoint method*. in *2018 AIAA Aerospace Sciences Meeting*. 2018.
- [28] Hersey, S., A. Sridharan, and R. Celi, *Multiobjective performance optimization of a coaxial compound rotorcraft configuration*. Journal of Aircraft, 2017. **54**(4): p. 1498-1507.
- [29] Imiela, M., *High-fidelity optimization framework for helicopter rotors*. Aerospace Science and Technology, 2012. **23**(1): p. 2-16.
- [30] Johnson, C. and G. Barakos. *Optimising aspects of rotor blades in forward flight*. in *49th AIAA aerospace sciences meeting including the new horizons forum and aerospace exposition*. 2011.
- [31] Leusink, D., D. Alfano, and P. Cinnella, *Multi-fidelity optimization strategy for the industrial aerodynamic design of helicopter rotor blades*. Aerospace Science and Technology, 2015. **42**: p. 136-147.
- [32] Zhu, Z. and Q.-j. Zhao, *Optimization for rotor blade-tip planform with low high-speed impulsive noise characteristics in forward flight*. Proceedings of the Institution of Mechanical Engineers, Part G: Journal of Aerospace Engineering, 2017. **231**(7): p. 1312-1324.
- [33] Elfarra, M., M. Kaya, and F. Kadioglu. *A parametric CFD study for the effect of spanwise parabolic chord distribution on the thrust of an untwisted helicopter rotor blade*. in *2018 AIAA Aerospace Sciences Meeting*. 2018.
- [34] Singh, P. and P.P. Friedmann, *A Computational Fluid Dynamics–Based Viscous Vortex Particle Method for Coaxial Rotor Interaction Calculations in Hover*. Journal of the American Helicopter Society, 2018. **63**(4): p. 1-13.

[35] Lewis, R.M., Virginia Torczon, and Michael W. Trosset., *Direct search methods: then and now*. Journal of computational and Applied Mathematics 124.1-2, 2000: p. 191-207..

[36] Shahmiri, F. and F. Saghafi, *Improvement of dynamic response prediction of helicopters*. Aircraft Engineering and Aerospace Technology, 2007.

[37] Shahmiri, F. and F. Saghafi, *Examination of indirect responses of helicopters using a refined inflow model*. Aircraft Engineering and Aerospace Technology, 2009.

[38] Pitt, D.M. and D.A. Peters, *Theoretical prediction of dynamic-inflow derivatives*. 1980.

[39] Peters, D.A., D.D. Boyd, and C.J. He, *Finite-state induced-flow model for rotors in hover and forward flight*. Journal of the American Helicopter Society, 1989. 34(4): p. 5-17.

[40] Eccles, D.M., *A Validation of the Joint Army/Navy Rotocraft Analysis and Design Software By Comparison With H-34 and UH-60A Flight Test*. 1995, NAVAL POSTGRADUATE SCHOOL MONTEREY CA.

[41] Turnour, S.R., *Flight dynamics simulation modeling for hingeless and bearingless rotor helicopters*. niversity of Maryland, 1996: p. College Park.

[42] Audet, C. and C. Tribes, *Mesh-based Nelder–Mead algorithm for inequality constrained optimization*. Computational Optimization and Applications, 2018. 71(2): p. 331-352.

[43] Montgomery, D.C., *Design and analysis of experiments*. 2017: John wiley & sons.

## Appendix A

Measured data of UH-60A helicopter in sea-level standard.

Design Parameters											Performance Response		
$V_\infty$ (Kts)	$W$ (lbs)	$c_0$ (ft)	$tr$	$trst$ (r/R)	$A_0$ (deg)	$A_1$ (deg)	$A_2$ (deg)	$\phi_1$ (deg)	$\phi_2$ (deg)	$2P$ $cos.$ (deg)	$C_T$	$C_P$	$L/D$
140	22000	3.5	0.4	0.9	-10	10	1	360	0	1	0.00701	0.000674	3.79
80	22000	1.5	0.6	0.6	-10	1	10	0	360	1	0.007535	0.000519	2.81
140	17500	3.5	0.6	0.6	-20	10	1	360	360	2	0.005463	0.000716	2.83
140	17500	1.5	0.4	0.6	-20	10	10	360	0	2	0.005427	0.000593	3.42
140	17500	1.5	0.6	0.6	-10	1	10	0	0	2	0.005421	0.000616	3.29
110	17500	2.5	0.5	0.75	-15	5.5	5.5	180	180	1.5	0.005709	0.000397	4.02
80	22000	1.5	0.4	0.6	-20	10	1	360	0	1	No trim available		
80	17500	3.5	0.6	0.9	-10	10	10	0	0	2	No trim available		
80	22000	3.5	0.4	0.9	-10	1	10	0	360	2	0.007537	0.000489	2.98
110	19750	2.5	0.5	0.75	-15	10	5.5	180	180	1.5	0.006503	0.000429	4.20
110	19750	1.5	0.5	0.75	-15	5.5	5.5	180	180	1.5	0.006503	0.000392	4.59
110	19750	2.5	0.5	0.75	-15	5.5	5.5	180	180	1.5	0.006503	0.000417	4.32
110	19750	2.5	0.5	0.75	-15	5.5	5.5	360	180	1.5	0.006505	0.000422	4.26
140	17500	3.5	0.6	0.9	-10	10	1	0	360	1	0.005435	0.000665	3.05
140	22000	1.5	0.4	0.9	-20	1	10	0	0	1	0.007009	0.00065	3.93
140	22000	1.5	0.4	0.9	-10	1	1	360	360	2	0.007001	0.000641	3.98
140	22000	1.5	0.6	0.9	-10	10	10	0	360	2	0.007006	0.000807	3.16
140	17500	1.5	0.4	0.9	-10	1	1	0	360	1	0.005416	0.000503	4.04
140	22000	3.5	0.6	0.6	-20	10	1	0	0	1	0.007033	0.000744	3.43
140	22000	3.5	0.4	0.6	-10	1	10	0	360	1	0.00702	0.000712	3.59
140	17500	1.5	0.4	0.9	-20	10	1	360	360	1	0.005423	0.000532	3.81
110	22000	2.5	0.5	0.75	-15	5.5	5.5	180	180	1.5	0.0073	0.000441	4.54
140	17500	3.5	0.6	0.6	-10	10	10	360	0	1	0.005447	0.000722	2.81
140	17500	1.5	0.4	0.6	-10	1	10	360	360	1	0.00542	0.000577	3.52
140	17500	3.5	0.4	0.9	-10	10	10	360	360	2	0.005451	0.000763	2.66
140	17500	3.5	0.4	0.9	-20	1	1	0	360	2	0.005462	0.000714	2.84
80	22000	3.5	0.4	0.6	-10	10	1	360	360	2	0.007536	0.000436	3.35

Design Parameters											Performance Response		
$V_\infty$ (Kts)	$W$ (lbs)	$c_0$ (ft)	$tr$	$trst$ (r/R)	$A_0$ (deg)	$A_1$ (deg)	$A_2$ (deg)	$\phi_1$ (deg)	$\phi_2$ (deg)	$2P$ $cos.$ (deg)	$C_T$	$C_P$	$L/D$
110	19750	2.5	0.5	0.75	-15	5.5	5.5	180	180	1	0.006503	0.000412	4.37
140	17500	3.5	0.6	0.9	-20	1	10	360	0	2	0.005489	0.000829	2.45
80	17500	3.5	0.6	0.6	-10	1	1	0	360	2	No trim available		
80	22000	1.5	0.4	0.6	-10	1	1	0	0	2	No trim available		
140	22000	1.5	0.6	0.9	-20	1	1	0	360	1	0.007006	0.000596	4.28
80	22000	3.5	0.6	0.9	-10	10	1	360	0	1	0.007537	0.000456	3.20
140	17500	1.5	0.6	0.6	-20	10	10	0	360	1	0.005428	0.000576	3.52
140	22000	3.5	0.6	0.6	-20	1	10	0	360	2	0.007049	0.000854	2.99
80	22000	3.5	0.6	0.6	-20	1	1	360	360	1	0.007537	0.000462	3.15
80	22000	1.5	0.6	0.6	-10	10	1	0	0	2	No trim available		
80	22000	3.5	0.6	0.6	-10	1	10	360	0	2	0.007537	0.000489	2.98
140	17500	1.5	0.6	0.9	-20	10	1	0	0	2	0.005425	0.000571	3.55
140	22000	3.5	0.4	0.9	-20	10	10	360	360	2	0.007052	0.00086	2.97
80	22000	3.5	0.4	0.6	-20	1	10	0	0	1	0.00754	0.000478	3.05
140	17500	1.5	0.4	0.6	-20	1	1	0	0	1	0.005422	0.000501	4.06
80	22000	3.5	0.6	0.6	-20	10	10	0	360	1	0.007542	0.000518	2.82
80	17500	1.5	0.4	0.6	-20	1	1	360	360	2	0.005939	0.000305	3.80
110	19750	3.5	0.5	0.75	-15	5.5	5.5	180	180	1.5	0.006506	0.000481	3.74
80	17500	3.5	0.4	0.6	-20	1	10	360	360	2	0.005946	0.000434	2.67
140	22000	3.5	0.6	0.9	-20	10	10	360	0	1	0.007052	0.000866	2.94
110	19750	2.5	0.5	0.75	-15	5.5	5.5	0	180	1.5	0.006505	0.000422	4.26
80	22000	1.5	0.4	0.6	-20	10	10	0	360	2	No trim available		
80	17500	1.5	0.6	0.9	-10	10	1	0	360	2	0.005939	0.000328	3.54
140	22000	3.5	0.6	0.9	-10	1	1	0	0	2	0.007016	0.000722	3.53
80	22000	1.5	0.6	0.9	-20	1	10	0	0	2	0.007536	0.000462	3.16
140	22000	1.5	0.6	0.6	-20	1	1	360	0	2	0.007006	0.000685	3.72
140	17500	1.5	0.4	0.6	-10	10	1	0	360	2	0.005416	0.000554	3.66
140	17500	3.5	0.4	0.9	-10	1	10	0	0	1	0.005446	0.000696	2.91
140	22000	1.5	0.6	0.6	-10	1	1	360	0	1	0.007001	0.00063	4.05
110	19750	2.5	0.5	0.9	-15	5.5	5.5	180	180	1.5	0.006504	0.000428	4.21
80	17500	1.5	0.4	0.6	-10	10	10	0	0	1	0.005939	0.000336	3.45
80	22000	3.5	0.6	0.9	-20	10	1	360	360	2	0.00754	0.000521	2.80
80	17500	1.5	0.6	0.6	-10	10	10	360	360	2	0.005939	0.000364	3.19
110	19750	2.5	0.5	0.75	-15	5.5	1	180	180	1.5	0.006505	0.00043	4.18
80	17500	1.5	0.4	0.9	-20	1	10	0	360	1	0.00594	0.000313	3.70
110	19750	2.5	0.5	0.6	-15	5.5	5.5	180	180	1.5	0.006503	0.000405	4.45
80	17500	3.5	0.6	0.9	-20	1	1	0	0	1	No trim available		
80	22000	1.5	0.4	0.9	-10	10	10	360	0	2	0.007535	0.000522	2.79
80	17500	3.5	0.6	0.9	-10	1	10	360	360	1	No trim available		
80	19750	2.5	0.5	0.75	-15	5.5	5.5	180	180	1.5	0.006737	0.000358	3.66
110	19750	2.5	0.5	0.75	-15	5.5	10	180	180	1.5	0.006503	0.000418	4.31

Design Parameters											Performance Response		
$V_\infty$ (Kts)	$W$ (lbs)	$c_0$ (ft)	$tr$	$trst$ (r/R)	$A_0$ (deg)	$A_1$ (deg)	$A_2$ (deg)	$\phi_1$ (deg)	$\phi_2$ (deg)	$2P$ $cos.$ (deg)	$C_T$	$C_P$	$L/D$
140	19750	2.5	0.5	0.75	-15	5.5	5.5	180	180	1.5	0.006213	0.000576	3.98
80	17500	3.5	0.4	0.9	-20	10	10	360	0	1	No trim available		
110	19750	2.5	0.5	0.75	-15	5.5	5.5	180	360	1.5	0.006506	0.000452	3.98
140	17500	1.5	0.6	0.9	-10	10	10	360	0	1	0.005422	0.000593	3.42
80	17500	3.5	0.4	0.6	-20	10	1	0	360	1	No trim available		
110	19750	2.5	0.5	0.75	-15	5.5	5.5	180	0	1.5	0.006506	0.000452	3.98
110	19750	2.5	0.5	0.75	-15	1	5.5	180	180	1.5	0.006505	0.000418	4.31
110	19750	2.5	0.4	0.75	-15	5.5	5.5	180	180	1.5	0.006503	0.000409	4.40
140	22000	3.5	0.4	0.6	-10	10	10	0	0	2	0.007024	0.00078	3.27
140	17500	3.5	0.4	0.6	-10	1	1	360	0	2	0.005427	0.00061	3.33
80	22000	3.5	0.4	0.9	-20	10	1	0	0	1	0.007539	0.000483	3.02
110	19750	2.5	0.5	0.75	-10	5.5	5.5	180	180	1.5	0.006503	0.000416	4.33
80	17500	3.5	0.4	0.9	-10	1	1	360	360	1	No trim available		
80	17500	3.5	0.4	0.6	-20	10	1	0	0	2	0.005944	0.000402	2.88
80	22000	1.5	0.4	0.9	-10	10	10	360	360	1	0.007535	0.000474	3.08
80	22000	1.5	0.4	0.9	-20	1	1	360	0	1	0.007535	0.000398	3.67
140	22000	1.5	0.6	0.6	-20	10	1	360	360	1	0.007006	0.000739	3.45
80	17500	1.5	0.6	0.9	-10	1	1	360	0	2	0.005939	0.000309	3.75
110	19750	2.5	0.5	0.75	-20	5.5	5.5	180	180	1.5	0.006506	0.000444	4.05
110	19750	2.5	0.5	0.75	-15	5.5	5.5	180	180	2	0.006505	0.000426	4.23
110	19750	2.5	0.6	0.75	-15	5.5	5.5	180	180	1.5	0.006504	0.000428	4.21
140	22000	1.5	0.6	0.9	-20	1	10	360	360	2	0.00701	0.000699	3.65
80	17500	1.5	0.6	0.6	-20	1	10	360	0	1	0.00594	0.000317	3.65

**COPYRIGHTS**

©2023 by the authors. Published by Iranian Aerospace Society This article is an open access article distributed under the terms and conditions of the Creative Commons Attribution 4.0 International <https://creativecommons.org/licenses/by/4.0/>